Physics in Medicine & Biology

PAPER • OPEN ACCESS

Dosimetry for repetitive transcranial magnetic stimulation: a translational study from Alzheimer's disease patients to controlled *in vitro* investigations

To cite this article: Francesca Camera *et al* 2024 *Phys. Med. Biol.* **69** 185001

IOP Publishing Phys. Med. Biol. 69 (2024) 185001 https://doi.org/10.1088/1361-6560/ad6f69

Physics in Medicine & Biology

IPEM Institute of Physics and Engineering in Medicine

OPEN ACCESS

RECEIVED
29 March 2024

REVISED
6 August 2024

ACCEPTED FOR PUBLICATION
14 August 2024

PUBLISHED
2 September 2024

PAPER

Dosimetry for repetitive transcranial magnetic stimulation: a translational study from Alzheimer's disease patients to controlled *in vitro* investigations

Francesca Camera[1], Eleonora Colantoni[2], Arianna Casciati[1], Barbara Tanno[1], Lucia Mencarelli[3], Francesco Di Lorenzo[3], Sonia Bonnì[3], Giacomo Koch[3] and Caterina Merla[1,*]

[1] Division of Biotechnologies, ENEA, Rome 00123, Italy
[2] Division of Sustainable Agri-Food Systems, ENEA, Rome 00123, Italy
[3] Department of Clinical and Behavioural Neurology, Santa Lucia Foundation IRCCS, Rome 00179, Italy
[*] Author to whom any correspondence should be addressed.

E-mail: caterina.merla@enea.it

Keywords: electromagnetic dosimetry, rTMS, Alzheimer's disease patients, *in vitro* system, induced electric field

Supplementary material for this article is available online

Abstract

Objective. Recent studies have indicated that repetitive transcranial magnetic stimulation (rTMS) could enhance cognition in Alzheimer's Disease (AD) patients, but to now the molecular-level interaction mechanisms driving this effect remain poorly understood. While cognitive scores have been the primary measure of rTMS effectiveness, employing molecular-based approaches could offer more precise treatment predictions and prognoses. To reach this goal, it is fundamental to assess the electric field (E-field) and the induced current densities (J) within the stimulated brain areas and to translate these values to *in vitro* systems specifically devoted in investigating molecular-based interactions of this stimulation. *Approach.* This paper offers a methodological procedure to guide dosimetric assessment to translate the E-field induced in humans (in a specific pilot study) into *in vitro* settings. Electromagnetic simulations on patients' head models and cellular holders were conducted to characterize exposure conditions and determine necessary adjustments for *in vitro* replication of the same dose delivered in humans using the same stimulating coil. *Main results.* Our study highlighted the levels of E-field and J induced in the target brain region and showed that the computed E-field and J were different among patients that underwent the treatment, so to replicate the exposure to the *in vitro* system, we have to consider a range of electric quantities as reference. To match the E-field to the levels calculated in patients' brains, an increase of at least the 25% in the coil feeding current is necessary when *in vitro* stimulations are performed. Conversely, to equalize current densities, modifications in the cells culture medium conductivity have to be implemented reducing it to one fifth of its value. *Significance.* This dosimetric assessment and subsequent experimental adjustments are essential to achieve controlled *in vitro* experiments to better understand rTMS effects on AD cognition. Dosimetry is a fundamental step for comparing the cognitive effects with those obtained by stimulating a cellular model at an equal dose rigorously evaluated.

1. Background

Transcranial magnetic stimulation (TMS) is a noninvasive technique used to modulate brain cortical activity and to study functional connectivity (Barker *et al* 1985). It applies local electromagnetic (EM) fields to those areas of the brain that are related to specific functions or pathological alterations to promote the modification of the neuronal connections (Barker *et al* 1985, Rossini *et al* 2015, Valero-Cabré *et al* 2017).

TMS is based on Faraday's law, where a rapidly changing electric current in a coil generates a magnetic (H) field that induces an electric (E) field in nearby conductive tissues, altering the electrical behavior of the neuronal cells composing the brain (Barker *et al* 1985).

TMS devices generate short (200–500 μs) but intense (1–2 T) pulses of H-field (Rossini *et al* 2015, Turi *et al* 2021, Drakaki *et al* 2022). Single pulse stimulation produces a short time response, whereas repetitive magnetic pulses stimulation, known as repetitive transcranial magnetic stimulation (rTMS), has more prolonged and complex effects on brain activity (Lefaucheur *et al* 2014, Huang *et al* 2017). Different or opposite effects can be obtained by changing stimulation properties such as the number of pulses, the rate of application, and the intensity of each rTMS stimulus (Chen *et al* 1997, Maeda *et al* 2000, Huang *et al* 2005, Rossini *et al* 2015).

However, the main differences in rTMS application for the treatment of neurological disorders lie in the diversity of stimulation target, for example: the primary motor cortex (M1) for the treatments of motor functions (Young *et al* 2014, Zhang *et al* 2022b), the dorsolateral prefrontal cortex for the treatment of depression (O'Reardon *et al* 2007, Levkovitz *et al* 2015) or for the modulation of cognitive functions (Lefaucheur *et al* 2014, Fisicaro *et al* 2019), the language areas in applications associated to language processing (Arheix-Parras *et al* 2021).

Notably, recent works showed that rTMS can be used to treat Alzheimer's Disease (AD) improving patients' cognition (Weiler *et al* 2020, Menardi *et al* 2022). In particular, in a clinical pilot study, Koch and co-authors demonstrated that long-term memory was significantly improved in mild AD patients stimulated with high frequency rTMS in the Precuneus area (PC) (Koch *et al* 2018, 2022). Each patient received the same stimulation pattern in terms of the number of pulses and repetition frequency; however, the intensity of the stimulation is patient-specific, and it corresponds to the resting motor threshold (RMT). Among different assessment strategies (Borckardt *et al* 2006, Tranulis *et al* 2006), this threshold has been defined as the lowest intensity producing motor-evoked potentials (MEPs) of >50 μV in at least five out of ten trials in the relaxed first dorsal intereosseous (FDI) muscle of the right hand (Rossini *et al* 2015).

Even if this clinical trial has shown therapeutic efficacy, very little is known about the biological mechanisms that occur at the cellular level in the exposed area bringing to such important clinical outcomes. Therefore, a deeper knowledge of these biological mechanisms would lead to more effective development of a new biomedical application of rTMS, as well as to the concrete possibility of controlling its efficacy in time.

To date, one research strategy to increase the knowledge of rTMS effects on brain activity down to the molecular level consists of performing experimental observations and specific molecular analysis in *in vitro* cellular models under controlled EM exposures (Post *et al* 1999, Rotem and Moses 2008, Grehl *et al* 2016, Tang *et al* 2016, Lenz *et al* 2016). To correlate clinical outcomes with *in vitro* exposure results, it is mandatory to deliver to the cells the same EM dose induced in humans. However, the delivery of defined rTMS conditions to the culture dishes resembling as much as possible the E-field strength in human brains is challenging. To achieve this goal, different choices were carried out involving both the design of mini figure-of-eight or mini coil specifically optimized to be adapted to culture conditions (Tang *et al* 2016, Grehl *et al* 2016). Another approach is to stimulate the cultured cells using clinical coils adopted for humans (Post *et al* 1999, Lenz *et al* 2016), which is the approach we decided to use in our investigation. In these previous studies, the selection of stimulation parameters used *in vitro* does not entail a direct translation to human exposure conditions. This limitation reduces the relevance of the results obtained.

Therefore, this paper aims to provide a methodological procedure to offer guidance for a dosimetric assessment when conducting *in vitro* experiments using the same stimulation coils of clinical TMS applications using specific protocols and stimulating targets.

In this context, E-field simulations play an essential role in linking *in vitro, in vivo* and clinical studies, with computational modeling increasingly employed to integrate experimental practices for assessing the efficacy of administered rTMS protocols (Gomez-Tames *et al* 2020, Shirinpour *et al* 2021). For this reason, non-specific voxel- and surface-based body models have been proposed in the literature (Gjonaj *et al* 2002, Makris *et al* 2008, Christ *et al* 2009, Findlay 2014, Iacono *et al* 2015, Noetscher *et al* 2021). However, employing a patient-specific head model rather than a generalized one to simulate the E-fields is the primary approach to achieve a quantitative measure of the stimulated EM dose for its translation *in vitro*.

To date, most of the EM simulations in biological tissues are done using a finite-element method (FEM) (Hiptmair 2002), that is implemented in many open-source environments that are compatible with patients' magnetic resonance images (MRI).

Numerical dosimetry for rTMS in human brain models is well investigated (Gomez-Tames *et al* 2020), especially for the cortical areas mentioned above. In our study, specific attention was given to the exposure conditions experienced by patients (Koch *et al* 2018, 2022), for which a dosimetric evaluation has not been performed so far.

We used dosimetric simulations using patients' specific head models MRI-derived to obtain the E-field and *J* values induced in the brain at these exposure conditions (Koch *et al* 2018, 2022). This step helps to determine the level of stimulation needed in *in vitro* system to obtain dosimetric values like those experienced by patients. Consequently, we obtained practical guidelines for optimizing the exposure design for future *in vitro* experiments that will be performed by our research group to clarify the molecular mechanisms underlying the cognitive enhancement observed in AD patients after rTMS treatment.

2. Materials and methods

2.1. The proposed methodological approach

Figure 1 presents a schematic representation of the methodological approach proposed in this paper for future controlled settings of *in vitro* experiments. Even if our attention has been focused on the pilot study previously published (Koch *et al* 2018, 2022), this proposed procedure is general and can be used in any other study when human stimulating coils are used for *in vitro* experiments.

To perform all the steps reported in figure 1, we (1) simulated nine patients' head models (Target A: head brain, figure 1) and an *in vitro* multi-well system (Target B: cells cultures, figure 1) to compute the E-field and *J* induced in the two targets, respectively Dose A and Dose B1 (figure 1). (2) We assessed the adjustments needed in the stimulation parameters to generate in the Target B an equivalent dose (Dose B2 = Dose A). These steps are preparatory for (3) comparing the effects induced by the exposure at an equivalent dose in the two systems. This final step will be addressed in future investigations by our group.

2.2. Numerical modeling of patients and the in vitro system

The medical device used to deliver rTMS consists in a generator of a pulsed current signal (DuoMAG XT, Deymed) that supplies an external figure-of-8 coil (Deymed 70BF). The signal used in the daily clinical stimulation is a short pulses sequence (Koch *et al* 2018). This sequence is composed of 40 trains of 40 pulses; each train lasts 2 s and between a train and another there are 28 s without signal, so the entire sequence lasts 20 min. The pulses in one train are bi-phasic and are delivered at a repetition frequency of 20 Hz, and the single pulse waveform is approximable to a sinusoid of 3200 Hz (R-square: 0.9976, figure 2). The intensity of the stimulation is patient-specific, and it corresponds to the 100% of the RMT defined as the lowest intensity producing MEPs of >50 μV in at least five out of ten trials in the relaxed FDI muscle of the right hand (Rossini *et al* 2015). Normally, for rTMS applications, the stimulation intensity is not given in terms of the coil's feeding current amplitude, but in terms of the percentage of the maximum stimulator output (MSO), and typical values for this application lie in the range between 50%–70% of MSO (Koch *et al* 2011). During the treatment, the coil is positioned over the PC with an orientation parallel to the midline with the handle pointing downward as illustrated in figure 1.

To evaluate the E-field induced in cerebral structures by rTMS, nine head models were developed using T1 and (when available) T2 MRI from the patients who underwent the treatment, whose stimulation intensity was known.

The MRI images have a spatial resolutionof 1 mm $\times$ 1 mm $\times$ 1 mm and they were segmented using the *charm* tool of SimNIBS v.4.0.0 (Thielscher *et al* 2015, Saturnino *et al* 2019, Puonti *et al* 2020), which, accounting for the heterogeneity of the head, grouped all tissues in nine anatomies: white matter (WM), grey matter (GM), cerebrospinal fluid (CSF), compact bone, spongy bone, scalp, eyeballs, blood and muscle (Wagner *et al* 2004, Gabriel *et al* 2009, Opitz *et al* 2015). SimNIBS is used in our computation being an open-source simulation package that integrates the MRI segmentation with mesh generation and quasi-static FEM E-field computation. We set the default vertex density of 0.5 nodes per mm^2. Some features of the resulting mesh for all head models are given in table 1.

The head meshes contained an average of $6.6 \pm 0.4 \times 10^5$ nodes, $1.1 \pm 0.1 \times 10^6$ triangles, $3.9 \pm 0.2 \times 10^6$ tetrahedra.

During head meshing, SimNIBS calculated transformations that were used to translate simulation results from patient's coordinates to standard spaces, such as the Montreal Neurological Institute space or FreeSurfer's FsAverage (https://surfer.nmr.mgh.harvard.edu). These coordinates refer to normalized spaces that are very useful when it is necessary to compare the anatomy of multiple human brains or compute group statistics (as we did to obtain analyses of figures 6 and 7).

Since the single pulse waveform is approximable by a sinusoid at 3200 Hz, that is in the low-frequency range, thus the quasi-static approximation holds. Under this approximation, the conduction currents are at least one order of magnitude higher than the displacement currents for most of the tissues (Barchanski *et al* 2005, De Santis *et al* 2012), and therefore the tissue conductivities were considered constant. We used the standard values from SimNIBS, i.e.: σ(WM) = 0.126 S m^{-1}, σ(GM) = 0.275 S m^{-1}, σ(CSF) = 1.654 S m^{-1}, σ (scalp) = 0.465 S m^{-1}, σ(compact bone) = 0.008 S m^{-1}, σ(spongy bone) = 0.025 S m^{-1},

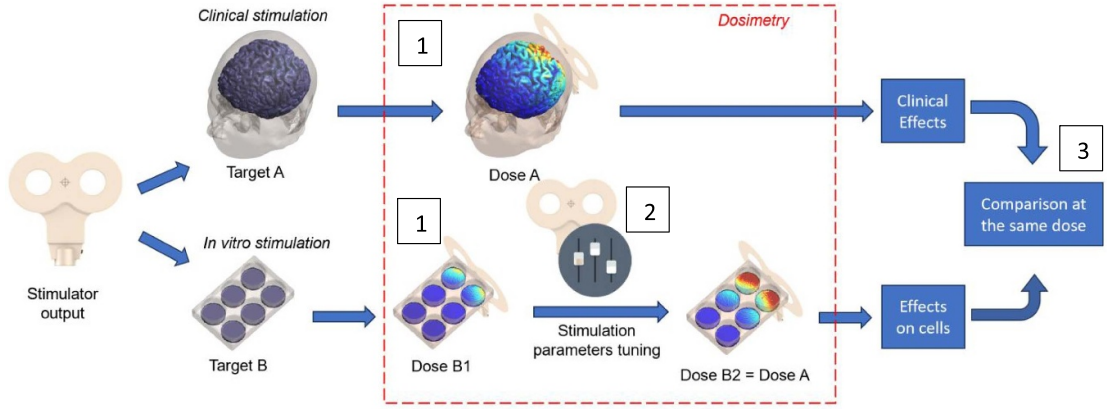

Figure 1. Schematic representation of the proposed methodological approach: (1) we utilize numerical simulations to calculate the electromagnetic (EM) dose induced by employing an identical stimulation protocol in two distinct scenarios: the clinical setting (Target A) and the *in vitro* experimental setup (Target B); (2) we assess the adjustments needed in the stimulation parameters to generate an equivalent dose in both systems; (3) the goal is to compare the effects of exposure at an equivalent dose in the two systems (this point is beyond the scope of this paper and it will be addressed in a future work).

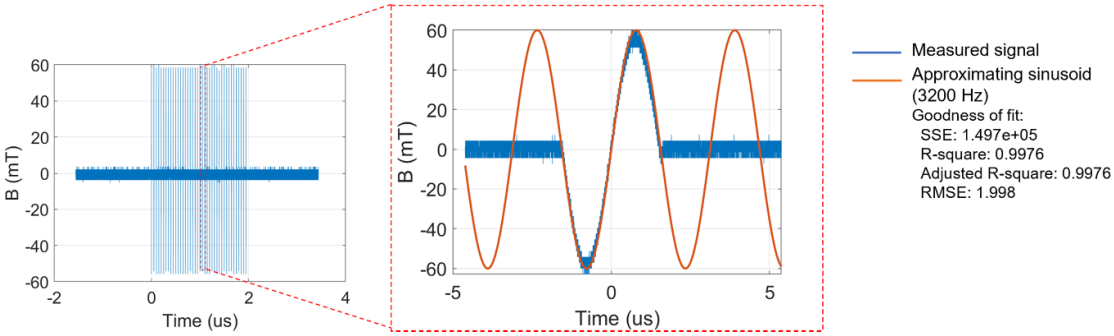

Figure 2. Pulses in the rTMS protocol. Left panel: one of the 40 trains that constitute the daily clinical stimulation (sampling rate: 10 us). Right panel: one of the 40 magnetic pulses contained in a train (sampling rate: 8 ns); the pulse is perfectly approximable by a sinusoidal signal of 3200 Hz. Measured signal was acquired using ELT-B-Field-Probe of 3 cm^2 (Narda, Savona, Italy) connected to an ELT-400 Exposure Level Tester (Narda, Savona, Italy).

Table 1. Mesh metrix for head models from nine patients.

Patient id	# nodes	# tetrahedra	# triangles	Mean tet. volume (mm^3)	Mean tet. edge (mm)
1	6.5×10^5	3.8×10^6	1.1×10^6	1.1 ± 4.5	1.9 ± 1.0
2	6.5×10^5	3.8×10^6	1.1×10^6	0.9 ± 4.0	1.7 ± 1.0
3	6.7×10^5	3.9×10^6	1.2×10^6	0.9 ± 4.2	1.8 ± 1.0
4	6.9×10^5	4.0×10^6	1.2×10^6	0.9 ± 3.8	1.8 ± 1.0
5	6.8×10^5	4.0×10^6	1.2×10^6	1.0 ± 4.7	1.8 ± 1.0
6	6.8×10^5	4.0×10^6	1.2×10^6	1.1 ± 4.9	1.9 ± 1.0
7	7.1×10^5	4.2×10^6	1.2×10^6	0.9 ± 3.7	1.8 ± 1.0
8	6.2×10^5	3.7×10^6	1.1×10^6	0.9 ± 4.2	1.8 ± 1.0
9	5.9×10^5	3.5×10^6	1.0×10^6	1.1 ± 4.6	2.0 ± 1.0

σ(eyeball) = 0.500 S m^{-1}, σ(blood) = 0.600 S m^{-1}, σ(muscle) = 0.160 S m^{-1} (Wagner *et al* 2004, Gabriel *et al* 2009, Opitz *et al* 2015). As already explained, at this frequency, the permittivity ($\varepsilon_r\varepsilon_0$) for all tissues is about 10^{-6} F m^{-1} or less, so, in this condition, displacement current can be neglected (Barchanski *et al* 2005, Gabriel *et al* 2009, De Santis *et al* 2012).

To position the figure-of-8 coil in the model as in the real clinical configuration, individual electroencephalography (EEG) coordinates were automatically calculated by SimNIBS software for all patients based on four fiducials points (inion Iz, nasion Nz, left preauricular point LPA, right preauricular point RPA), to obtain the 10–10 EEG positions (Jurcak *et al* 2007). After tuning the current intensity for human simulations, the coil was properly positioned in the Pz position (10–10 EEG standard) (Jurcak *et al*

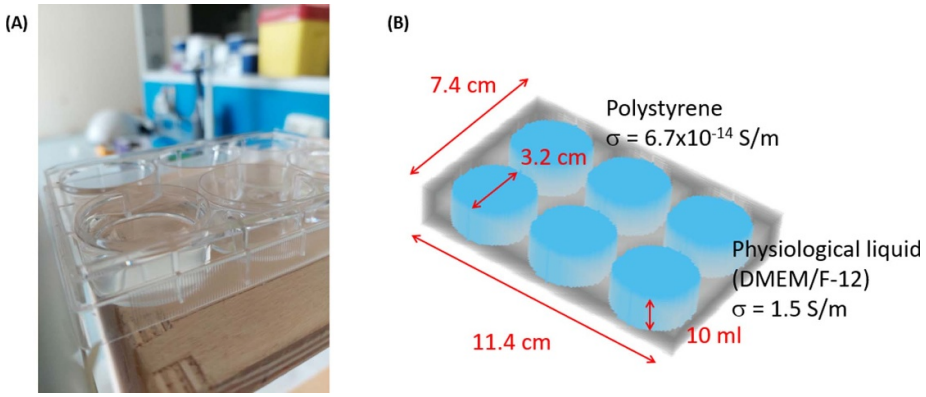

Figure 3. Representation of the cellular holder. (A) Picture of six multi-well for *in vitro* stimulations and (B) the multi-well EM model.

2007), which is the one that can be projected on the PC. The coil has been positioned 4 mm away from the scalp and tangentially oriented to it.

The built-in SimNIBS model of the Deymed 70BF figure-of-8 coil was chosen as the TMS coil for the simulations. For all the built-in coils models in SimNIBS, the stimulation intensity is given in terms of dI/dt, that is the rate of change of the coil current. From the paper (Drakaki *et al* 2022) we obtained the relationship between the stimulation intensity expressed in % MSO (Koch *et al* 2018, 2022) and the input for SimNIBS in dI/dt. Values for each analyzed patient are here reported in table 2.

Finally, the cellular holder was modeled. This is a six-multi-well plate (Corning, Somerville, MA, USA) typically used in biological studies, that is a rectangular polystyrene ($\sigma = 6.7 \times 10^{-14}$ S m^{-1}) support measuring 7.4 cm $\times$ 11.4 cm, which contains six cylindrical wells, each 1.7 cm in height and with a radius of 1.6 cm, with walls approximately 2 mm thick (figure 3). Since for future *in vitro* study we chose the cellular model for AD described in de Medeiros *et al* (2019), dealing with a 2D cell culture, each cylinder was filled with a culture medium with a conductivity of $\sigma = 1.5$ S m^{-1}, which represents the conductivity of the medium experimentally used to maintain cells in culture i.e. the Dulbecco's Modified Eagle's Medium /Nutrient Mixture F-12 (DMEM/F-12, Thermo Fisher Scientific, Waltham, MA, USA). The volume of 10 ml of cells culture medium was chosen with preliminary simulations to maximize energy transfer and obtain a higher E-field on the floor of the wells (see figures S1–S4 in supplementary material). This cell holder was designed using Matlab R2019b by creating a 3D grid of 300 $\times$ 300 $\times$ 300 mm^3 with a resolution of 1 mm^3. Each point in this grid was assigned a numerical label depending on whether the point was occupied by air, polystyrene, or fluid. This labeled volume was imported as a nii.gz file into SimNIBS and meshed with the *meshmesh* tool that is built in the software. The final mesh was composed by 2.57 $\times$ 10^4 nodes and 1.33 $\times$ 10^5 tetrahedrons with a mean edge size of about 2 mm.

We simulated four different relative positions between the multi-well and the stimulation coil (figure 4) to find the best experimental setup among the different possibilities of orientation. It is possible to choose the coil orientation and position adapting its affine transformation matrix with respect the geometrical model imported. We used two different positions in which the coil plane was parallel to the floor of the wells (Position B and C), and other two different positions in which the coil axis was parallel to the floor of the wells (Position A and D). The chosen stimulation intensity was set to 60% MSO, which was an average value of the ones delivered to patients. For all positions, the coil was placed adjacent (distance from the holder = 0 mm) to the cell holder to ensure that this experimental setup was reproducible and repeatable under actual exposure conditions.

3. Results

3.1. Numerical dosimetry of patients' head

Multiple E-field features were evaluated for all simulated head models. In table 2, we reported the E-field and volumetric features in the brain structures (GM and WM respectively). First, for each model, the maximum value of the E-field both in the GM (E_{maxGM}) and in the WM (E_{maxWM}) was obtained by taking the 99.9th percentile of the distribution in each anatomical regions (GM and WM), to avoid numerical artifacts (Gubernati *et al* 2022, Camera *et al* 2024). This first analysis permitted to identify the brain region in which the induced E-field reaches the maximum (for details on the maximum values in each material, refer to table S1 in supplementary material). The rationale behind this choice is related to the biological reasons, as the

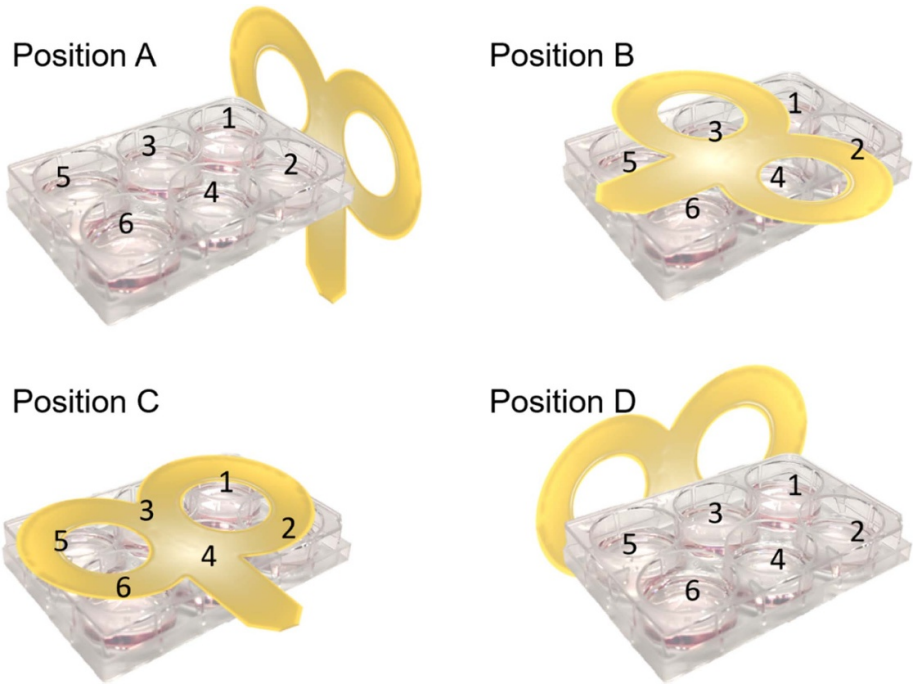

Figure 4. Representation of different simulated relative positions between the coil and the multi-well. Four different positions were tested: two with the coil plane parallel to the well floor (Position B and C) and two with the coil axis parallel to the well floor (Position A and B).

in vitro model (monolayer of neuronal cell lines) cannot fully replicate the characteristics of either GM or WM. Then, the global maximum E-field (E_{max}) was set equal to the maximum between the two values. Finally, all the E-field values higher than E_{max} were considered equal to it. Since many authors (Gomez-Tames *et al* 2020, Drakaki *et al* 2022) take the brain volume exposed to an E-field equal to or greater than 50% of E_{max} to quantify focality, we considered this Vol_{50} (expressed in cm^3) as the stimulated volume. For our purposes, defining a stimulated volume is essential to identify an average electric quantity for comparing with the *in vitro* dosimetry results.

In that volume, we also calculated the averaged E-field (E_{mean}) and the averaged J (J_{mean}) weighted with the tetrahedrons volume, with the respective standard deviations (std) and coefficient of variation (CV = std/mean). We also indicated the percentage of GM and WM of the Vol_{50}.

E_{max} reached in the brain models ranges from 48.3 V m^{-1} to 74.7 V m^{-1}, while the E_{mean} is from 32.4 V m^{-1} to 49.0 V m^{-1}. In figure 5 we reported E_{max} (panel A) and E_{mean} (panel B) values as functions of the % MSO. It is possible to notice that the results' variability depends on the intensity of the coil's feeding current that ranges from 47% to 65% MSO, but it is also evident that the induced E-field and J depend also on individual patient anatomy, as different values are achieved for different patients' head models using the same % MSO. This highlights the need for personalized dosimetry for optimized rTMS treatments.

Table 2 also shows that about 35%–50% of the stimulated volume is composed of WM (see column 6), while, as a consequence, complementary percentage values of the stimulated volume are composed of GM (see column 5). Due to the different conductivities of WM and GM, the J (calculated as $J = \sigma E$) has consequently a greater variability than the E-field in the same volume. This is confirmed by the fact that the CV for E-field is lower than the CV for J.

To deepen the J variability, we reported in table 3 some further results obtained considering the two different brain regions, i.e. WM and GM.

In table 3 we can see that J ranges from 3.0 A m^{-2} (J_{min} in WM, column 6, patients 4) to 15.7 A m^{-2} (J_{max} in WM, column 7, patient 5) in WM and from 6.6 A m^{-2} (J_{min} in GM, column 3, patient 4) to 20.5 A m^{-2} (J_{max} in GM, column 4, patient 2) in GM. The averaged values in the two brain regions (J_{mean}) are also shown (columns 2 and 5). Results show that the variability for this quantity is quite high.

Finally, we analyzed simulations results also in the common FreeSurfer's FsAverage space. This space is a normalized one and it is composed of a surface located in the middle of the GM layer, on which SimNIBS remaps the E-field simulation results. Moreover, SimNIBS can assign labels to this FsAverage brain template referring to a specific atlas (Destrieux *et al* 2010). This gives us a rough estimation of the E-field induced by stimulation on the PC and the other brain areas that are reached by stimulation.

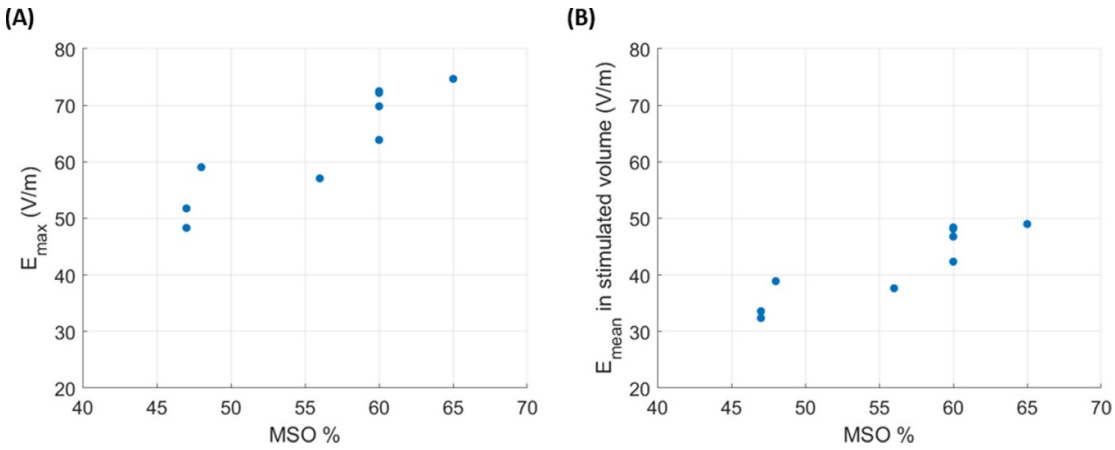

Figure 5. Relationship between the stimulation intensity and electric field. (A) E_{max} and (B) E_{mean} in the stimulated volume.

Table 2. EM and volumetric features obtained from simulations of the nine patients' head models. Simulations of the nine patients' heads, whose stimulation intensities (% MSO), on the basis of the pilot study in Koch *et al* (2018), (2022), are here reported for each analyzed patient, were converted in dI/dt and used to calculate the maximum E-field (E_{max}), the volume exposed to E-field equal to or greater than 50% of E_{max} (Vol_{50}), the percentage of the grey matter (GM) and the white matter (WM) in Vol_{50}, the E-field (E_{mean}) and the current densities (J_{mean}) averaged in Vol_{50} with standard deviations and coefficients of variation (CV).

Patient id	% MSO	dI/dt (A us^{-1})	E_{max} (V m^{-1})	Vol_{50} (cm^3)	% of GM in Vol_{50}	% of WM in Vol_{50}	E_{mean} (V m^{-1})	CV_E	J_{mean} (A m^{-2})	CV_J
1	48%	48.5	59.1	27.1	60%	40%	38.9 ± 8.3	0.2	8.4 ± 3.5	0.4
2	65%	65.7	74.7	33.5	60%	40%	49.0 ± 9.6	0.2	10.7 ± 4.4	0.4
3	60%	60.7	69.8	33.2	61%	39%	46.8 ± 9.4	0.2	10.2 ± 4.1	0.4
4	47%	47.5	48.3	45.7	50%	50%	32.4 ± 6.3	0.2	6.6 ± 2.9	0.4
5	56%	56.6	57.1	40.5	62%	38%	37.6 ± 7.6	0.2	8.3 ± 3.4	0.4
6	60%	60.7	72.2	34.7	64%	36%	48.2 ± 9.9	0.2	10.7 ± 4.2	0.4
7	60%	60.7	72.5	40.0	61%	39%	48.4 ± 9.5	0.2	10.6 ± 4.4	0.4
8	60%	60.7	63.9	37.6	61%	39%	42.4 ± 8.5	0.2	9.2 ± 3.8	0.4
9	47%	47.5	51.8	25.8	52%	48%	33.6 ± 6.8	0.2	6.8 ± 2.8	0.4

Table 3. Current densities for all patients' head models in Vol_{50}.

Patient id	J_{mean} (A m^{-2})	J_{min} in GM (A m^{-2})	J_{max} in GM (A m^{-2})	J_{mean} in GM (A m^{-2})	J_{min} in WM (A m^{-2})	J_{max} in WM (A m^{-2})	J_{mean} in WM (A m^{-2})
1	8.4 ± 3.5	8.1	16.2	10.8 ± 2.2	3.7	12.1	4.9 ± 1.3
2	10.7 ± 4.4	10.3	20.5	13.7 ± 2.7	4.7	12.1	6.0 ± 1.2
3	10.2 ± 4.1	9.6	19.2	13.0 ± 2.6	4.4	10.3	5.8 ± 1.2
4	6.6 ± 2.9	6.6	13.3	9.1 ± 1.8	3.0	7.1	4.0 ± 0.7
5	8.3 ± 3.4	7.8	15.7	10.5 ± 2.1	3.6	15.7	4.7 ± 1.0
6	10.7 ± 4.2	9.9	19.8	13.3 ± 2.7	4.5	10.8	6.0 ± 1.3
7	10.6 ± 4.4	10.0	19.9	13.6 ± 2.7	4.6	13.6	5.9 ± 1.1
8	9.2 ± 3.8	8.8	17.6	11.8 ± 2.4	4.0	11.8	5.2 ± 1.1
9	6.8 ± 2.8	7.1	12.9	9.2 ± 1.7	3.3	10.9	4.3 ± 1.0

In figure 6 we showed the E-field distribution on the left hemisphere PC (results obtained on the right hemisphere are comparable). This distribution was obtained by averaging results over the nine patients' simulations normalized to the maximum induced E-field. Although the E-field normalization can make quantitative considerations more difficult, it allows us to estimate which brain areas are involved and to what extent by the described rTMS protocol.

Figure 7 shows the brain areas that are exposed to the normalized E-field equal to or greater than 50% of E_{max} averaging the results among all the patients. The region of PC receives an intense E-field values (see figure 6), but other areas nearby are also reached by the stimulation.

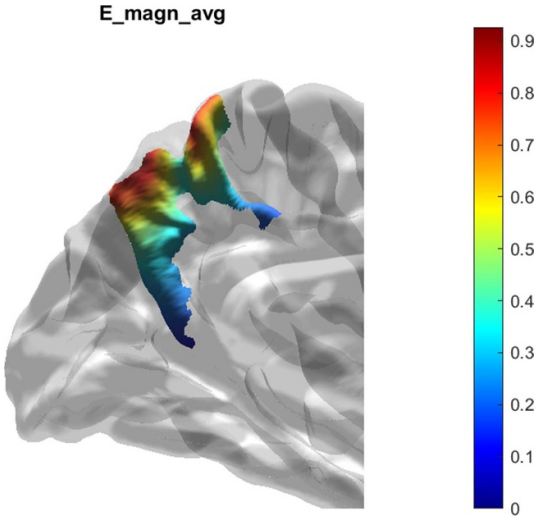

Figure 6. Averaged normalized E-field among nine patients' head models on left PC area.

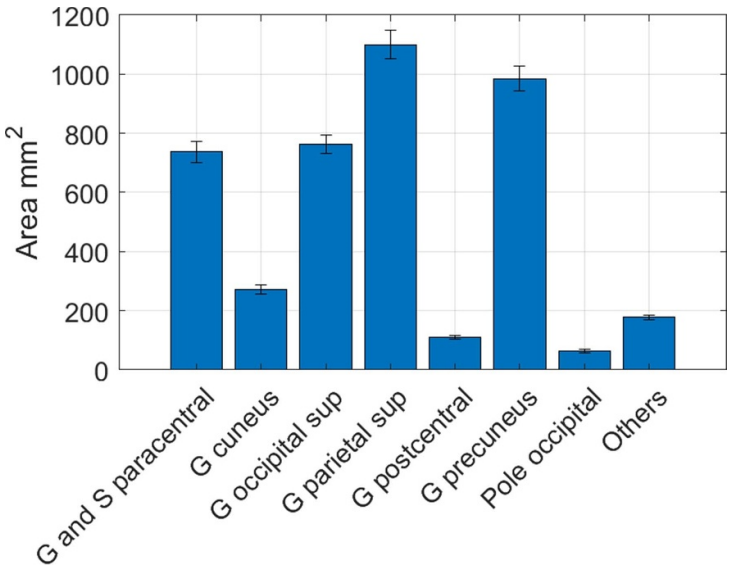

Figure 7. Brain areas reached by rTMS stimulation. Areas reached by stimulation (averaged among nine patients) referring to the specific atlas by Destrieux *et al* (2010) using the protocol detailed in the section Methods 'Numerical modeling of patients and in vitro system'.

3.2. Numerical dosimetry of the in vitro system

During our *in vitro* experiments, cells will be preliminarily plated to attach as monolayer to the floor of the wells. So, only simulation results on this plane are here considered.

As for the brain, we considered as stimulated area the one in which the E-field is equal to or higher than the half of the maximum obtained for all the exposure conditions.

In figure 8(A), we reported the E_{mean} values (obtained by averaging the E-field induced in the stimulated area) and in figure 8(B) the vectorial normalized to maximum E-field distribution obtained on the floor of all the six wells for all the four simulated positions at 60% MSO (see table 4 for the maximum values). Since the DMEM was homogeneous with a conductivity $\sigma = 1.5$ S m^{-1}, the induced J was simply obtained as the product of σ and E-field.

Induced J can reach averaged values in the more exposed wells that range from 45 (in position A) to 63 A m^{-2} (in position B), higher than the ones obtained in patients' brain of the order of 10 and 5 for averaged values for WM and GM respectively; as a general consideration, J in wells is comparable with J in brains only when the E-field is very low, even an order of magnitude less than the one induced in the stimulated volume of the brain. In table 4 the averaged E-field (E_{mean}) and J (J_{mean}) in these stimulated areas are summarized.

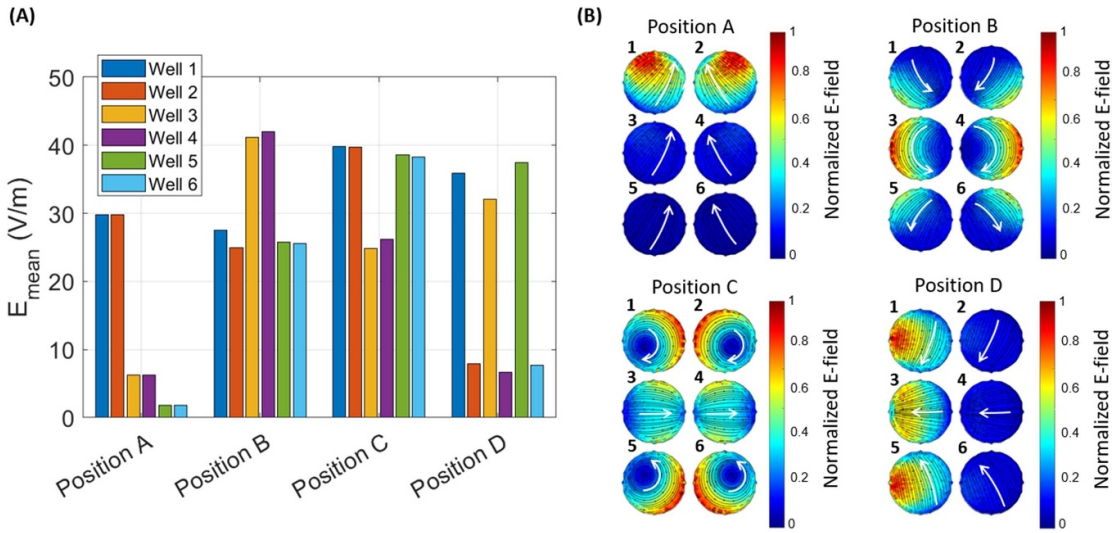

Figure 8. E-field intensity and distribution. (A) Averaged E-field (E_{mean}) calculated in the stimulated area of each well of the plate in the four different relative positions between coil and multi-well (see figure 4) at 60% MSO and (B) normalized E-field distributions obtained on the floor of all the six wells for all the four simulated positions at 60% MSO. The black lines indicate the direction of the electric field vector at each point, while the white arrows denote its orientation.

Table 4. Averaged E-field (E_{mean}) and J (J_{mean}) calculated in the stimulated area of the wells, for all the different exposure conditions.

Position	Well with max E-field	E_{mean} (V m^{-1})	E_{max} (V m^{-1})	J_{mean} (A m^{-2})
A	*1,2*	29.8 ± 5.5	44.3	44.7 ± 8.2
B	*3,4*	42.0 ± 7.1	63.8	63.0 ± 10.7
C	*1,2,5,6*	39.8 ± 7.0	58.6	59.8 ± 10.5
D	*1,5*	37.5 ± 5.8	56.9	56.2 ± 8.7

We can see that the E_{mean} in the stimulated area (column 3, table 4) is comparable with the one induced in patients' brains (that ranges from 32.4 to 49.0 V m^{-1}, see table 2), the only position in which it is slightly lower is the positions A. On the contrary, the J values in the wells are significantly higher than the corresponding brain values, both in terms of maximum and average values (see table 3). It is, therefore, necessary to adjust certain experimental parameters to produce equivalent electric signals (E-field and J) in cell models corresponding to human brain stimulations.

Parallel coil plane positions (positions B and C, figures 4 and 8) maximize the induced E-field but the E-field distribution is predominantly concentrated along the edges of the well. While in the other positions (parallel to the coil axis, positions A and D, figures 4 and 8) the E-field homogeneity is higher.

In figure 9 the E-field distribution on the floor of two wells is depicted, showcasing the maximum E-field reached for two different relative positions between the coil and the multi-well (position A and B, see figures 4 and 8). In position A (blue data), where the floor of the well aligns parallel to the coil axis, the distribution appears more concentrated, signifying a more uniform spread of E-field values in contrast to the other position. In the other position, the distribution appears broader, leading to a higher inhomogeneity of the induced E-field values.

Overall, these findings indicate that coil position has to be chosen in agreement with the specific focus of the *in vitro* experiments at maximizing the homogeneity or the amplitude of the E-field and J.

4. Discussion

With the goal of deepening the changes induced by magnetic stimulation at the cellular level to better comprehend the molecular mechanisms activated by rTMS, we aimed to translate clinical rTMS treatment into an *in vitro* AD cellular model. To achieve this and to gain insights into the effects observed in clinical practice, it is crucial to administer the same EM dose to the investigated cell model.

Therefore, quantifying the dose induced in both systems (clinical and *in vitro*) is mandatory to select the most appropriate stimulation protocol for the AD cellular model, considering the possibility of optimizing the stimulation intensity and the relative coil position to the wells hosting the cells.

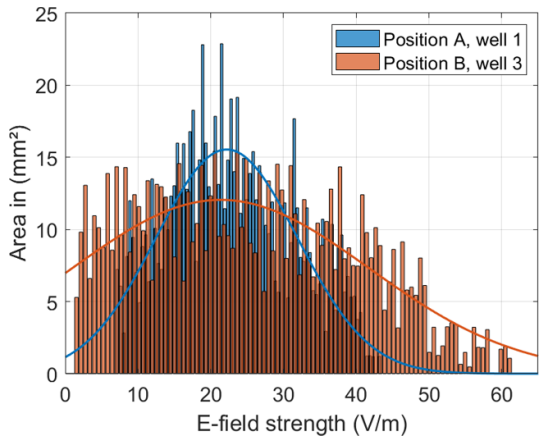

Figure 9. E-field distribution on the floor of two wells in which the maximum E-field is reached for two different relative positions between coil and multi-well. In the position A (blu data), in which the floor of the well is parallel to the coil axis, the distribution is more concentrated, indicating that the E-field values are more uniform compared to the other position, where the distribution is broader, resulting in a greater inhomogeneity of the E-field values.

In the last years, many numerical dosimetric studies have been already conducted employing realistically segmented human head models derived from MRI data (Gomez-Tames *et al* 2020, Tzirini *et al* 2022). The primary objective of these investigations has been to explore the variability of the induced E-field due to the inter-subject anatomical variations or to the targeted stimulated brain region, or to know the best simulation settings for numerically accurate E-field calculation (Gomez *et al* 2020, Zhang *et al* 2022a). Only few previous studies have combined the individualized E-field modeling with experimental TMS to ensure uniform dosing across participants in a clinical trial (Beynel *et al* 2020), to optimize TMS coil placement (Deng *et al* 2023) or to investigate the relationships between the calculated E-field and measured motor thresholds (Laakso *et al* 2018). To our knowledge, no one has related patients' and treatment specific dosimetry to study the best conditions to replicate the patients' dose *in vitro*. We would like to point out that to maximally improve the accuracy of the dosimetric results it would be preferable to use both T1 and T2 images for segmentation and it is important to carefully inspecting head meshes when using FEMs for dosimetry.

Our results confirm that differences in anatomical head morphology influence the induced E-field. This is evident among patients who underwent the same stimulation intensity (patients 3, 6, 7, and 8) but received varying doses. E_{max} reached in the brain models ranges from 48.3 V m^{-1} to 74.7 V m^{-1}, while the E_{mean} from 32.4 V m^{-1} to 49.0 V m^{-1}, depending on the patient and on the intensity of the coil's feeding current. Instead, J ranges from 3.0 A m^{-2} to 15.7 A m^{-2} in WM and from 6.6 A m^{-2} to 20.5 A m^{-2} in GM. Furthermore, the physiological response, from which the treatment intensity is selected (Koch *et al* 2018, 2022) varies significantly among all patients. This variability can be due to many factors, such as age, sex, disease severity, other comorbidities, and synaptic plasticity impairment (Francesco and Di Lorenzo F and Koch G 2021). Consequently, for this clinical application, there is no single value for the E-field and J that can be representative of the treatment. This suggests that patient-tailoired dosimetry is increasingly desirable to understand TMS mechanisms and enhance treatment efficacy. On the other hand, it indicates that, when designing *in vitro* experiments, there is a range of values that need to be considered to make comparisons. The choice of the Vol_{50} including both GM and WM is specific for the application of this dosimetry, which is the definition of comparable parameters for 2D cells culture. So, considering GM and WM separately can be somewhat limiting, given that *in vitro* cells are all of the same type, and they do not represent neither the GM nor the WM in a specific way. However, the 2D model chosen for our future experiments is a well-accepted model for AD (de Medeiros *et al* 2019) able to reproduce the impairment of the pathology and to show the improvements obtained after the TMS treatments.

Our dosimetry on patients' PC indicates that, even though this small area receives an intense E-field, the brain areas engaged by the stimulation extends beyond the PC, however confined into the surrounding areas which are part of the parietal cortex known to be involved in the neurodegenerative process of AD since the earliest phases.

Dosimetry on multi-well, performed in this work, reveals that the E-field levels induced on the floor of the wells, where the cells are plated, are comparable to the averaged E-field values obtained in the human head model. In the *in vitro* system, once maximized the cell culture medium volume, these averaged quantities range from 30 to 42 V m^{-1} for E-field and from 45 to 63 A m^{-2} for J, depending on the coil's relative position to the six-well plate. The results of dosimetry, as it is well known, are strongly dependent on

the geometry and electrical characteristics of the systems described, so stimulating the *in vitro* system with the same coil at the same distance of the GM is not a suitable criterium to guarantee comparable exposure. Therefore, after selecting a reproducible setup, we assured that, at the chosen distance, cells can reach the same exposure to E and *J* as in the clinical stimulations. Conductivity variability is another issue to be taken into account in future studies to better evaluate E-field distribution in a statistical way. However, the procedure described in figure 1 and that we suggest to follow for tuning *in vitro* experiments, remains still valid.

In this paper, we analyzed some possible positions (the more practical for experimental purposes and the one that maximize the tangential E-field at the floor of the wells) of the coil with respect to the multi-well plate, achieving better homogeneity of the field distributions in positions A and D (figure 4) for the same exposure system (coil) used in the clinical pilot study. This choice of using patients' stimulating coil is extremely convenient from an experimental point of view. However, in a future study following the procedure described here, it would be possible to design a specific coil for the *in vitro* system to further improve field homogeneity and levels, even if only in a limited number of wells in a multi-well plate.

In fact, achieving comparable E-field homogeneity among the different wells of a multi-well plate when using a single focal coil is very challenging. To reach this goal, multiple coils would be needed, which would significantly complicate the generation chain for the *in vitro* experiments.

Notably, positions maximizing the induced E-field level in the six-well plate determine an E-field distribution with lower values into the well center, where cells maximally grow. Hence, a position ensuring E-field uniformity in the center, as in A and D in figure 8 might be preferable, even if the induced E-field is slightly lower. We focalized our attention in maximizing the tangential E-field at the floor of the wells, as we deal with a 2D *in vitro* model, however different field orientation can be foreseen, especially in those application where 3D models are considered and where neuronal network activation become a relevant endpoint.

4.1. Practical guidelines for tuning in vitro experiments

On the bases of our results, to achieve a suitable trade-off between patients' exposure and *in vitro* exposure the stimulation intensities need to be tuned, opting for higher values of the % MSO in *in vitro* experiments compared to the clinical ones.

On the other hand, the conductivity of the typical medium used to maintain cells *in vitro* is higher than that of brain tissues. This leads to simulating higher *J* in the *in vitro* model than those induced in the human brain model. If tuning the E-field, as described previously, involves increasing the stimulation intensities, the current densities would largely surpass those of the human brain. Therefore, these authors suggest to modifying the buffer for cell stimulation to decrease its conductivity while maintaining an osmolarity compatible with cell survival and an equal E-field.

Lastly, it is crucial to highlight that our procedure is entirely general and applicable to different types of *in vitro* systems, such as multi-well plates with a higher number of wells, as well as single petri dishes of various dimensions. A similar approach can even be applied to mouse models to investigate molecular pathways modulated following rTMS. These types of studies and dosimetric assessments represent the next steps in our research effort.

5. Conclusions

Numerical models derived from patients' MRI brain scans have been developed and utilized to simulate PC stimulation using a commercial coil employed in rTMS. Additionally, a dosimetric model of an *in vitro* system was developed, employing the same coil used in clinical treatments positioned in various arrangements relative to a typical six-well plate.

Our results emphasize variability in the averaged values of the E-field reached in human brain models, primarily influenced by different patient-dependent stimulation intensities.

Our simulations of the *in vitro* system also shown that specific coil positions maximize the induced E-field, but the distribution highlights that the minimum E-field is reached in the center of the well, where cells typically grow, significantly reducing exposure homogeneity—a fundamental requirement for *in vitro* exposure.

Our findings suggest that adjustments are needed for the *in vitro* system to be exposed to a dose comparable to that experienced by brain cells in the PC and neighboring regions. If the E-field has to remain consistent with all the induced levels, the coil feeding current must be slightly increased and using coil positioning to the six-well plate enabling the maximization of the induced E-field and its homogeneity

(i.e. position A or D). Conversely, to equalize current densities, modifications in buffer conductivity should be considered to decrease currents inside the wells. This information is crucial for establishing an appropriate *in vitro* stimulation protocol to elicit comparable exposure to that in patients' brains and investigate potential molecular mechanisms underlying the observed cognitive improvements in rTMS-treated AD patients.

Data availability statement

The data cannot be made publicly available upon publication because they contain sensitive personal information. The data that support the findings of this study are available upon reasonable request from the authors.

Acknowledgments

The authors want to thank Dr Rosanna Pinto and Alessandro Zambotti for their support in B-field measurements on the stimulating coil system.

Ethics statement

The clinical trial providing patients' MRI has been approved by the Ethics Committee of the Santa Lucia Foundation CE/PROG.716, Rome, Italy. All patients entering the study provided written informed consensus.

Fundings

This work was supported by 'Progetti gruppi di ricerca 2020' Regione Lazio POR FESR Lazio 2014-2020 n. A0375-2020-36546, *Dosimetria di un nuovo trattamento rTMS in colture 3d della malattia di Alzheimer per l'identificazione di marcatori di efficacia terapeutica—DTA*- CUP I8F21000950009.

ORCID iDs

Francesca Camera https://orcid.org/0000-0001-6455-4094
Eleonora Colantoni https://orcid.org/0000-0003-1301-2492
Arianna Casciati https://orcid.org/0000-0003-2487-3060
Barbara Tanno https://orcid.org/0000-0001-6098-699X
Lucia Mencarelli https://orcid.org/0000-0002-4006-4629
Francesco Di Lorenzo https://orcid.org/0000-0001-9871-229X
Sonia Bonnì https://orcid.org/0000-0002-1780-4131
Giacomo Koch https://orcid.org/0000-0001-6155-9439
Caterina Merla https://orcid.org/0000-0001-8612-9566

References

Arheix-Parras S, Barrios C, Python G, Cogné M, Sibon I, Engelhardt M, Dehail P, Cassoudesalle H, Moucheboeuf G and Glize B 2021 A systematic review of repetitive transcranial magnetic stimulation in aphasia rehabilitation: leads for future studies *Neurosci. Biobehav. Rev.* **127** 212–41

Barchanski A, Gersem H D, Gjonaj E and Weiland T 2005 Impact of the displacement current on low-frequency electromagnetic fields computed using high-resolution anatomy models *Phys. Med. Biol.* **50** N243

Barker A T, Jalinous R and Freeston E I L 1985 Non-invasive magnetic stimulation of human motor cortex *Lancet* **325** 1106–7

Beynel L *et al* 2020 Site-specific effects of online rTMS during a working memory task in healthy older adults *Brain Sci.* **10** 5

Borckardt J J, Nahas Z, Koola J and George M S 2006 Estimating resting motor thresholds in transcranial magnetic stimulation research and practice: a computer simulation evaluation of best methods *J. ECT* **22** 169

Camera F, Merla C and De Santis E V 2024 Comparison of transcranial magnetic stimulation dosimetry between structured and unstructured grids using different solvers *Bioengineering* **11** 7

Chen R, Classen J, Gerloff C, Celnik P, Wassermann E M, Hallett M and Cohen L G 1997 Depression of motor cortex excitability by low-frequency transcranial magnetic stimulation *Neurology* **48** 1398–403

Christ A *et al* 2009 The virtual family—development of surface-based anatomical models of two adults and two children for dosimetric simulations *Phys. Med. Biol.* **55** N23

Consultato FreeSurfer—an overview | ScienceDirect topics (available at: www.sciencedirect.com/topics/medicine-and-dentistry/freesurfer) (Accessed 15 febbraio 2024)

de Medeiros L M *et al* 2019 Cholinergic differentiation of human neuroblastoma SH-SY5Y cell line and its potential use as an *in vitro* model for Alzheimer's disease studies *Mol. Neurobiol.* **56** 7355–67

De Santis V, Douglas M, Kuster N and Chen X L 2012 Impact of the skin conductivity and displacement currents on LF numerical dosimetry *Int. Symp. on Electromagnetic Compatibility—EMC EUROPE* (IEEE) pp 1–4

Deng Z-D, Robins P L, Dannhauer M, Haugen L M, Port J D and Croarkin E P E 2023 Optimizing TMS coil placement approaches for targeting the dorsolateral prefrontal cortex in depressed adolescents: an electric field modeling study *Biomedicines* **11** 8

Destrieux C, Fischl B, Dale A and Halgren E E 2010 Automatic parcellation of human cortical gyri and sulci using standard anatomical nomenclature *NeuroImage* **53** 1–15
Di Lorenzo F and Koch G 2021 Synaptic impairment: the new battlefield of Alzheimer's disease *Alzheimers Dement.* **17** 314–5
Drakaki M, Mathiesen C, Siebner H R, Madsen K and Thielscher A 2022 Database of 25 validated coil models for electric field simulations for TMS *Brain Stimul.* **15** 697–706
Findlay R P 2014 Induced electric fields in the MAXWEL surface-based human model from exposure to external low frequency electric fields *Radiat. Prot. Dosim.* **162** 244–53
Fisicaro F, Lanza G, Grasso A A, Pennisi G, Bella R, Paulus W and Pennisi M 2019 Repetitive transcranial magnetic stimulation in stroke rehabilitation: review of the current evidence and pitfalls *Ther. Adv. Neurol. Disord.* **12** 1756286419878317
Gabriel C, Peyman A and Grant E H 2009 Electrical conductivity of tissue at frequencies below 1 MHz *Phys. Med. Biol.* **54** 4863–78
Gjonaj E, Bartsch M, Clemens M, Schupp S and Weiland E T 2002 High-resolution human anatomy models for advanced electromagnetic field computations *IEEE Trans. Magn.* **38** 357–60
Gomez L J, Dannhauer M, Koponen L M and Peterchev E A V 2020 Conditions for numerically accurate TMS electric field simulation *Brain Stimul.* **13** 157–66
Gomez-Tames J, Laakso I and Hirata A 2020 Review on biophysical modelling and simulation studies for transcranial magnetic stimulation *Phys. Med. Biol.* **65** 24TR03
Grehl S, Martina D, Goyenvalle C, Deng Z-D, Rodger J and Sherrard R M 2016 *In vitro* magnetic stimulation: a simple stimulation device to deliver defined low intensity electromagnetic fields *Front. Neural Circuits* **10** 85
Gubernati A C, Freschi F, Giaccone L and Scorretti E R 2022 Analysis of numerical artifacts using tetrahedral meshes in low frequency numerical dosimetry *Appl. Sci.* **12** 13
Hiptmair R 2002 Finite elements in computational electromagnetism *Acta Numer.* **11** 237–339
Huang Y-Z *et al* 2017 Plasticity induced by non-invasive transcranial brain stimulation: a position paper *Clin. Neurophysiol.* **128** 2318–29
Huang Y-Z, Edwards M J, Rounis E, Bhatia K P and Rothwell J C 2005 Theta burst stimulation of the human Motor Cortex *Neuron* **45** 201–6
Iacono M I *et al* 2015 MIDA: a multimodal imaging-based detailed anatomical model of the human head and neck *PLoS One* **10** e0124126
Jurcak V, Tsuzuki D and Dan E I 2007 10/20, 10/10, and 10/5 systems revisited: their validity as relative head-surface-based positioning systems *NeuroImage* **34** 1600–11
Koch G *et al* 2018 Transcranial magnetic stimulation of the precuneus enhances memory and neural activity in prodromal Alzheimer's disease *Neuroimage* **169** 302–11
Koch G *et al* 2022 Precuneus magnetic stimulation for Alzheimer's disease: a randomized, sham-controlled trial *Brain* **145** 3776–86
Koch G, Esposito Z, Kusayanagi H, Monteleone F, Codecá C, Di Lorenzo F, Caltagirone C, Bernardi G and Martorana A 2011 CSF tau levels influence cortical plasticity in Alzheimer's disease patients *J. Alzheimers Dis.* **26** 181–6
Laakso I, Murakami T, Hirata A and Ugawa E Y 2018 Where and what TMS activates: experiments and modeling *Brain Stimul.* **11** 166–74
Lefaucheur J-P *et al* 2014 Evidence-based guidelines on the therapeutic use of repetitive transcranial magnetic stimulation (rTMS) *Clin. Neurophysiol.* **125** 2150–206
Lenz M, Galanis C, Müller-Dahlhaus F, Opitz A, Wierenga C J, Szabó G, Ziemann U, Deller T, Funke K and Vlachos A 2016 Repetitive magnetic stimulation induces plasticity of inhibitory synapses *Nat. Commun.* **7** 10020
Levkovitz Y *et al* 2015 Efficacy and safety of deep transcranial magnetic stimulation for major depression: a prospective multicenter randomized controlled trial *World Psychiatry* **14** 64–73
Maeda F, Keenan J P, Tormos J M, Topka H and Pascual-Leone A 2000 Modulation of corticospinal excitability by repetitive transcranial magnetic stimulation *Clin. Neurophysiol.* **111** 800–5
Makris N, Angelone L, Tulloch S, Sorg S, Kaiser J, Kennedy D and Bonmassar G 2008 MRI-based anatomical model of the human head for specific absorption rate mapping *Med. Biol. Eng. Comput.* **46** 1239–51
Menardi A, Dotti L, Ambrosini E and Vallesi A 2022 Transcranial magnetic stimulation treatment in Alzheimer's disease: a meta-analysis of its efficacy as a function of protocol characteristics and degree of personalization *J. Neurol.* **269** 5283–301
Noetscher G M, Serano P, Wartman W A, Fujimoto K, Makarov S N and Zubair M 2021 Visible human project® female surface based computational phantom (Nelly) for radio-frequency safety evaluation in MRI coils *PLoS One* **16** e0260922
O'Reardon J P *et al* 2007 Efficacy and safety of transcranial magnetic stimulation in the acute treatment of major depression: a multisite randomized controlled trial *Biol. Psychiatry* **62** 1208–16
Opitz A, Paulus W, Will S, Antunes A and Thielscher A 2015 Determinants of the electric field during transcranial direct current stimulation *NeuroImage* **109** 140–50
Post A, Müller M B, Engelmann M and Keck M E 1999 Repetitive transcranial magnetic stimulation in rats: evidence for a neuroprotective effect in vitro and in vivo *Eur. J. Neurosci.* **11** 3247–54
Puonti O, Van Leemput K, Saturnino G B, Siebner H R, Madsen K H and Thielscher A 2020 Accurate and robust whole-head segmentation from magnetic resonance images for individualized head modeling *NeuroImage* **219** 117044
Rossini P M *et al* 2015 Non-invasive electrical and magnetic stimulation of the brain, spinal cord, roots and peripheral nerves: basic principles and procedures for routine clinical and research application. An updated report from an I.F.C.N. Committee *Clin. Neurophysiol.* **126** 1071–107
Rotem A and Moses E 2008 Magnetic stimulation of one-dimensional neuronal cultures *Biophys. J.* **94** 5065–78
Saturnino G B, Puonti O, Nielsen J D, Antonenko D, Madsen K H and Thielscher A 2019 SimNIBS 2.1: a comprehensive pipeline for individualized electric field modelling for transcranial brain stimulation *Brain and Human Body Modeling: Computational Human Modeling at EMBC 2018* ed S Makarov, M Horner, E G Noetscher and A C Di (Springer International Publishing) pp 3–25
Shirinpour S, Hananeia N, Rosado J, Tran H, Galanis C, Vlachos A, Jedlicka P, Queisser G and Opitz A 2021 Multi-scale modeling toolbox for single neuron and subcellular activity under transcranial magnetic stimulation *Brain Stimul.* **14** 1470–82
Tang R, Zhang G, Weng X, Han Y, Lang Y, Zhao Y, Zhao X, Wang K, Lin Q and Wang C 2016 *In Vitro* assessment reveals parameters-dependent modulation on excitability and functional connectivity of cerebellar slice by repetitive transcranial magnetic stimulation *Sci. Rep.* **6** 23420
Thielscher A, Antunes A and Saturnino E G B 2015 Field modeling for transcranial magnetic stimulation: a useful tool to understand the physiological effects of TMS? *2015 37th Annual Int. Conf. IEEE Engineering in Medicine and Biology Society (EMBC)* (IEEE) pp 222–5
Tranulis C, Guéguen B, Pham-Scottez A, Vacheron M N, Cabelguen G, Costantini A, Valero G and Galinovski A 2006 Motor threshold in transcranial magnetic stimulation: comparison of three estimation methods *Neurophysiol. Clin./Clin. Neurophysiol.* **36** 1–7

Turi Z, Normann C, Domschke K and Vlachos A 2021 Transcranial magnetic stimulation in psychiatry: is there a need for electric field standardization? *Front. Hum. Neurosci.* **15** 639640

Tzirini M, Chatzikyriakou E, Kouskouras K, Foroglou N, Samaras T and Kimiskidis E V K 2022 Electric field distribution induced by TMS: differences due to anatomical variation *Appl. Sci.* **12** 4509

Valero-Cabré A, Amengual J L, Stengel C, Pascual-Leone A and Coubard E O A 2017 Transcranial magnetic stimulation in basic and clinical neuroscience: a comprehensive review of fundamental principles and novel insights *Neurosci. Biobehav. Rev.* **83** 381–404

Wagner T A, Zahn M, Grodzinsky A J and Pascual-Leone A 2004 Three-dimensional head model simulation of transcranial magnetic stimulation *IEEE Trans. Biomed. Eng.* **51** 1586–98

Weiler M, Stieger K C, Long J M and Rapp P R 2020 Transcranial magnetic stimulation in Alzheimer's disease: are we ready? *eNeuro* **7** ENEURO.0235–19.2019

Young N A, Sharma M and Deogaonkar M 2014 Transcranial magnetic stimulation for chronic pain *Neurosurg. Clin. North Am.* **25** 819–32

Zhang H, Gomez L J and Guilleminot E J 2022a Uncertainty quantification of TMS simulations considering MRI segmentation errors *J. Neural Eng.* **19** 026022

Zhang W, Deng B, Xie F, Zhou H, Guo J-F, Jiang H, Sim A, Tang B and Wang Q 2022b Efficacy of repetitive transcranial magnetic stimulation in Parkinson's disease: a systematic review and meta-analysis of randomised controlled trials *eClinicalMedicine* **52** 101589